



UNIVERSITY OF LEEDS

This is a repository copy of *Carbon dioxide injection and associated hydraulic fracturing of reservoir formations*.

White Rose Research Online URL for this paper:
<http://eprints.whiterose.ac.uk/81441/>

Version: Accepted Version

Article:

Eshiet, KI and Sheng, Y (2013) Carbon dioxide injection and associated hydraulic fracturing of reservoir formations. *Environmental Earth Sciences*, 72 (4). 1011 - 1024.
ISSN 1866-6280

<https://doi.org/10.1007/s12665-013-3018-3>

Reuse

Unless indicated otherwise, fulltext items are protected by copyright with all rights reserved. The copyright exception in section 29 of the Copyright, Designs and Patents Act 1988 allows the making of a single copy solely for the purpose of non-commercial research or private study within the limits of fair dealing. The publisher or other rights-holder may allow further reproduction and re-use of this version - refer to the White Rose Research Online record for this item. Where records identify the publisher as the copyright holder, users can verify any specific terms of use on the publisher's website.

Takedown

If you consider content in White Rose Research Online to be in breach of UK law, please notify us by emailing eprints@whiterose.ac.uk including the URL of the record and the reason for the withdrawal request.



eprints@whiterose.ac.uk
<https://eprints.whiterose.ac.uk/>

Carbon dioxide Injection and Associated Hydraulic Fracturing of Reservoir Formations

Kenneth Imo-Imo Eshiet¹, Yong Sheng²

School of Civil Engineering
University of Leeds, LS2 9JT, Leeds, United Kingdom
E-mail: k.i.i.eshiet@leeds.ac.uk
E-mail: y.sheng@leeds.ac.uk

Abstract

The storage potential of subsurface geological systems makes them viable candidates for long term disposal of significant quantities of CO₂. The geo-mechanical responses of these systems as a result of injection processes as well as the protracted storage of CO₂ are aspects that require sufficient understanding. A hypothetical model has been developed that conceptualises a typical well-reservoir system comprising an injection well where the fluid (CO₂) is introduced and a production/abandoned well sited at a distant location. This was accomplished by adopting a numerical methodology (Discrete Element Method), specifically designed to investigate the geo-mechanical phenomena whereby the various processes are monitored at the inter-particle scale. Fracturing events were simulated. In addition, the influence of certain operating variables such as injection flow rate and fluid pressure was studied with particular interest in the nature of occurring fractures and trend of propagation, the pattern and magnitude of pressure build-up at the well vicinity, pressure distribution between well regions and pore velocity distribution between well regions.

Modelling results generally show an initiation of fracturing caused by tensile failure of the rock material at the region of fluid injection; however, fracturing caused by shear failure becomes more dominant at the later stage of injection. Furthermore, isolated fracturing events were observed to occur at the production/abandoned wells that were not propagated from the injection point. This highlights the potential of CO₂ introduced through an injection well, which could be used to enhance oil/gas recovery at a distant production well. The rate and magnitude of fracture development is directly influenced by the fluid injection rate. Likewise, the magnitude of pressure build-up is greatly affected by the fluid injection rate and the distance from the point of injection. The DEM modelling technique illustrated provides an effective procedure that allows for more specific investigations of geo-mechanical mechanisms occurring at sub-surface systems. The application of this

² Corresponding Author:
Address: School of Civil Engineering, University of Leeds, UK
e-mail: y.sheng@leeds.ac.uk

methodology to the injection and storage of CO₂ facilitates the understanding of the fracturing phenomenon as well as the various factors governing the process.

Key words: Hydraulic Fracturing, CO₂ Injection, Geological Storage

1.0 Introduction

The option of subsurface storage of CO₂ has been considered viable enough to attract significant attention. Uncertainties involved in the process have necessitated wide interest in the various phenomena, comprising but not limited to the following areas: monitoring of the fate of CO₂ once injected (Class et al., 2009, Eigestad et al., 2009, Lindeberg and Bergmo, 2003, Nordbotten et al., 2005a, Nordbotten et al., 2005b, Nordbotten et al., 2009, Pruess, 2008a, Pruess, 2008b, Xu et al., 2006); reservoir containment and capacity estimation (Bachu et al., 2007, Bradshaw et al., 2007, Kopp et al., 2009, Liao and Shangguan, 2009, Nunez-Lopez et al., 2008, Okwen et al., 2010, Wei and Saaf, 2009, Zhou et al., 2008); pressure build-up (Birkholzer et al., 2009, Mathias et al., 2009b, Rutqvist et al., 2007, Rutqvist et al., 2008, Streit and Hillis, 2004, Streit, 2002) and for brine formations, fluid displacement (Nicot et al., 2009, Nicot, 2008). Other areas of concern comprise geochemical/chemical issues such as changes in fluid composition following the injection of CO₂ (Huq et al., 2012) and diagenesis due to fluid-rock interactions (Beyer et al., 2012, Lucia et al., 2012, Pudlo et al., 2012). Potential areas for CO₂ storage include depleted oil and gas reservoirs, coal bed seams and deep saline formations. Also, the environmental and geo-mechanical benefits of CO₂ injection and storage have been extended to processes such as enhanced oil recovery (EOR) (Bachu et al., 2004, Godec et al., 2013, Gozalpour et al., 2005) enhanced gas recovery (EGR) (Al-Hashami et al., 2005, Hou et al., 2012, Kühn et al., 2012) and enhanced coal bed methane production (ECBM) (Pini et al., 2011, Zhang and Song, 2012).

Storage of CO₂ in subsurface systems involves transmitting the fluid into the desired formation depth. The rate of injection should be such that will not offset the stability of the system; however, the introduction of fluid will lead to an increase in the formation pressure, which without proper monitoring and control may result in mechanical failure of the material. As indicated in Bauer et al. (2012) and Park et al. (2012), tracking pressure development as the CO₂ is being injected and during post-mortem periods is essential in ensuring safety limits are not exceeded. An alternative measure of the evolution of fluid pressure can be achieved via changes in in-situ stress conditions. In order to

accomplish this Lempp et al. (2012) highlighted the possibility of developing an effective monitoring device that could be used for assessing changing stress conditions due to CO₂ storage. Alterations in stress/pore pressure conditions have various geo-mechanical consequences, an obvious one being the occurrence of fracturing events that may ultimately, if extensively propagated, lead to leakages.

Thermal effects including changes in in-situ reservoir temperature arising from heat transfer/exchanges between the injected CO₂ and the formation, contribute to the dynamics of underground activities (Hou et al., 2012, Norden et al., 2012, Singh et al., 2012). Changes in reservoir temperature are dependent on the geological structure and variations in rock thermal conductivity (Norden et al., 2012); some aspects of Joule-Thompson cooling (JTC) and viscous heat dissipation (VHD) are illustrated in Singh et al. (2012), while in Hou et al. (2012) the thermal process is incorporated with hydro-mechanical processes for the prediction of reservoir responses.

The interest in hydraulic fracturing is mainly because of its economic importance. It involves the initiation and subsequent propagation of fractures within rock formations and has been exploited extensively by the oil and gas industry to improve reservoir productivity. Hydraulic fracturing may occur naturally, when the minimum principal stress drops low and/or the fluid pressure becomes sufficiently high; moreover, it could be intentionally caused by injecting fluid into rocks at high velocities such that the fluid pressure within the rock exceeds the sum of the rock tensile strength and the minimum principal stress (Fjaer et al., 2008).

The process of hydraulic fracturing is quite complex and several studies have been undertaken in an attempt to improve the understanding of the phenomenon.. Theoretical and experimental investigations have been foremost in existing studies (Athavale and Miskimins, 2008, Blair et al., 1989, Casas et al., 2006, Daneshy, 1976, Daneshy, 1978, Elwood and Moore, 2009, Hanson et al., 1982, Hanson et al., 1981, Ishida, 2001, Ishida et al., 2004, Matsunaga et al., 1993, McLennan et al., 1986, Medlin and Masse, 1984, Murdoch, 1993a, Murdoch, 1993b, Murdoch, 1993c, Parrish et al., 1981, Teufel and Clark, 1984, Warpinski et al., 1982). For instance, Daneshy (1976) was able to draw an inference between some rock properties and the amount of pressure required for fracture extension, thereby establishing the term '*fracturability index*'; Daneshy (1978) determined the effect of the strength of the interface between layered rock formations, as well as their relative mechanical properties on the pattern of fracturing; Murdoch (1993a, 1993b, 1993c) carried out laboratory experiments and theoretical analysis to monitor pressure development and fracture propagation in soils; and more recently Athavale (2008) compared patterns of hydraulic fracturing between laminated (layered) and homogeneous materials.

The advent of developments in numerical techniques have prompted more studies (Al-Busaidi et al., 2005, Alqahtani and Miskimins, 2010, Boone and Ingraffea, 1990, Boutt et al., 2007, Boutt et al., 2011, Casas et al., 2006, Dean and Schmidt, 2009, El Shamy and Zeghal, 2005, Hoffman and Chang, 2009, Jansen et al., 2008, Lam and Cleary, 1986, Lujun et al., 2009, Papanastasiou, 1997, Rungamornrat et al., 2005, Shimizu et al., 2009, Shimizu et al., 2011, Warpinski et al., 1982, Yamamoto et al., 1999, Yew and Liu, 1993); these have added flexibility that complement field/laboratory experiments which, on their own, have limited and controlled conditions. Examples of the application of numerical methods include the finite element modelling technique used by Alqahtani and Miskimins (2010) to determine the stress distribution caused by the application of predefined sets of triaxial stresses on layered block systems (in order to simulate laboratory experiments) and the use of finite difference techniques by Hoffman and Chang (2009) to model hydraulically fractured wells and predict productivity. In addition, Dean and Schmidt (2009) illustrated the capability of a multiphase/multi-component modelling technique that couples hydraulic fracturing with other processes such as flow through porous media, heat convection and conduction, solids deposition and poroelastic/ poroplastic deformation.

Considering the phenomenon at the particle level, attempts have been made to study fluid-solid interactions including hydraulic fracturing by coupling DEM techniques with continuum methods of modelling fluid dynamics. This has been applied in the study of hydraulic fracturing (Eshiet et al., 2013), in sand production problems (Boutt et al., 2011), in studying the behaviour of sandy deposits when subjected to fluid flow (El Shamy and Zeghal, 2005) and to simulate simple cases of natural hydraulic fracture propagation (Boutt et al., 2007). Also, DEM techniques incorporating embedded fluid flow algorithms have been used to model acoustic emissions (AE) during studies of hydraulic fracturing (Al-Busaidi et al., 2005) and to investigate effects of viscosity and particle size distribution (Shimizu et al., 2011). In this approach the material is first characterised at the particle level before being scaled up to comprise of particle assemblies with dimensions and resolutions dependent on the geometric size of the phenomenon to be investigated. The formation material is characterised as an assembly of interacting discrete particles with inter-particle bond breakage and particle separation representing crack formation and cavity initiation respectively.

This study explores the DEM technique and extends its application to a simplified reservoir scale model consisting of an injection well and a far reach production/abandoned well within a homogeneous formation. The fluid (CO₂) - rock material interactions are scrutinised and more specifically fracturing events as a result of fluid flow rate and the pore pressure build up are examined.

2.0 Simulation procedure

2.1 Mechanics of particle assembly

The applied modelling formulation consists of a coupled DEM-CFD (Computational Fluid Dynamics) scheme, implemented via PFC2D (Particle Flow Code) (Itasca Consulting Group, 2008). The method simulates the mechanical behaviour of a collection of particles that may vary in size and shape. The term particle as used here represents a finite entity that occupies space and although the particles can be displaced independently, they interact with each other through contacts. The mechanical behaviour is thus portrayed with respect to the displacement of particles and the forces existing at the position of inter-particle contact. The particles are regarded as rigid bodies connected through contacts, and the extent of overlap between particles is associated to the contact force by the force displacement law. Newton's law of motion form the basis that relates forces with the resulting motion of particles. Where bond exist at contact between particles, the bond can only be broken when the bond strength is exceeded by inter-particle forces. The model dynamics is depicted via calculations using a timestepping algorithm that assumes within each time step a constant velocity and acceleration, with the timestep set to very small values such that vibrations form a given particle do not propagate further than the closest particles.

Particle behaviour is governed by two basic laws: the law of force-displacement and the law of motion. The force-displacement law defines the contact force between two entities in terms of their stiffness and the relative displacement between the entities. The contact force F_i is resolved into normal and shear components. This is given as (Itasca Consulting Group, 2008):

$$\vec{F}_i = \vec{F}_i^n + \vec{F}_i^s \quad (1a)$$

\vec{F}_i^n and \vec{F}_i^s is the normal and shear component vectors, respectively.

The normal contact force vector is given by

$$\vec{F}_i^n = K^n \vec{U}_i^n \quad (1b)$$

Where, K^n is the normal stiffness and \vec{U}_i^n is the displacement.

The shear contact force is calculated incrementally and is determined as the sum of the old shear force vector at the start of the timestep ($\{\vec{F}_i^s\}_{rot2}$), after rotation to account for motion of the contact plane, and the shear elastic force-increment vector ($\Delta\vec{F}_i^s$).

The new shear contact force is then given as

$$\vec{F}_i^s = \{\vec{F}_i^s\}_{rot2} + \Delta\vec{F}_i^s \quad (1c)$$

$$\Delta\vec{F}_i^s = -k^s \Delta\vec{U}_i^s \quad (1d)$$

Where, k^s is the shear stiffness at the contact, expressed as a tangent modulus and $\Delta\vec{U}_i^s$ is the shear component of the contact displacement increment within the timestep, Δt .

The movement of particles is determined by applying the law of motion to obtain the resultant force and moment acting on each particle. Thus, movement is described in terms of the translational displacement of the particle position and the rotation of the particle. The law of motion comprises two equations. Translational motion is expressed in vector form as

$$\vec{F}_i = m(\vec{\ddot{x}}_i - \vec{g}_i) \quad (2)$$

Where, \vec{F}_i is the resultant of all external forces acting on the particle; m is the particle mass, $\vec{\ddot{x}}_i$ is the particle acceleration and \vec{g}_i is the body force acceleration, such as due to gravity. For rotational motion the resultant moment \vec{M}_i acting on a particle is equated to the angular momentum \vec{H}_i of the particle, given as

$$\vec{M}_i = \vec{H}_i \quad (3)$$

2.2 Fluid flow coupling algorithm

To account for fluid flow CFD was coupled with DEM using a fixed coarse grid scheme that solves locally averaged two-phase mass momentum equations for the fluid velocity and pressure, presented as a generalised form of the Navier-Stokes equation modified to account for fluid-solid interaction. Although the grid scheme models fluid flow as a continuum, it supports the simulation of fluid-solid interaction which is done by overlaying the particle assembly by the fluid grid system. Timesteps for

the two overlapping schemes are managed such that the mechanical timestep used for particle motion is considerably greater than the fluid timestep.

The Navier-Stokes equation is modified to account for two-phase (solid-fluid) flow, assuming an incompressible fluid phase with constant density. It is expressed as

$$\rho_f \frac{\partial \epsilon \vec{v}}{\partial t} + \rho_f \vec{v} \cdot \nabla (\epsilon \vec{v}) = -\epsilon \nabla p + \mu_f \nabla^2 (\epsilon \vec{v}) + \vec{f}_b \quad (4)$$

The continuity equation (conservation of mass) equation is

$$\frac{\partial \epsilon}{\partial t} + \nabla \cdot (\epsilon \vec{v}) = 0 \quad (5)$$

Where, ρ_f is the fluid density, ϵ is the porosity, \vec{v} is the interstitial velocity, p is the fluid pressure, μ_f is the dynamic viscosity of the fluid and \vec{f}_b is the body force per unit volume. Fluid-particle interaction forces are described via the forces applied by particles on fluid and vice versa. The drag force (body force per unit volume experienced by the fluid) exerted by particles on the fluid is

$$\vec{f}_b = \beta \vec{u} \quad (6)$$

Where, β is the fluid-particle friction coefficient and \vec{u} is the average relative velocity between fluid and particles. In response an equal and opposite force is applied by each fluid element on particles in proportion to the volume of each particle. This drag force, for each particle, is given as

$$\vec{f}_{drag} = \frac{4}{3} \pi R^3 \frac{\vec{f}_b}{(1 - \epsilon)} \quad (7)$$

Considering the force due to buoyancy, the total force exerted by fluid on a particle is

$$\vec{f}_{fluid} = \vec{f}_{drag} + \frac{4}{3} \pi R^3 \rho_f \vec{g} \quad (8)$$

Where, R is the particle radius and \vec{g} is the acceleration due to gravity.

Apart from the distinct problem definition, the numerical methodology employed here differentiates this work from those presented in Eshiet and Sheng (2013). The major differences lie in the mode by which fluid flow is incorporated within the DEM particle assembly. In Eshiet and Sheng (2013) a fully coupled technique that involves an embedment of the flow of a deformable fluid within a particle assembly was applied. This has several advantages, such as the ability to adapt the flow domain to irregular geometries and configurations, the ability to apply flow parameters, for instance, pressure at remote points and along irregular configurations. It also handles strong pressure gradients

effectively. Computation of fluid parameters are not based on the continuum approach since the fluid domain is fully embodied and discretised along with the DEM particles.

This work illustrates a field scale application of the numerical procedure presented in Eshiet et al. (2013) where fluid flow is accounted for via a fixed coarse-grid fluid scheme that solves relevant fluid flow equations to derive cell averaged quantities of pressure and velocity. The equations governing fluid flow (Continuity and Navier-Stokes equations) are solved numerically by the finite difference method to determine the pressure and fluid velocity vector at each cell. Computation of fluid parameters is based on the continuum approach and the fluid domain is independently discretised using a grid system superimposed on the particle assembly. The advantages of this method include flexibility in settings and adjustments of the grid and boundary conditions of the fluid domain which can be made to align with the particle assembly, relative ease in monitoring and extracting values of fluid flow variables, such as fluid pressure and fluid velocity, and the display of fluid velocity vectors. The use of any coupling method depends on the research objective.

2.3 Modelling conditions

Model geometry loading

The model geometric dimension is 8 m x 12 m, scaled to represent a reservoir system consisting of an injection well close to the left boundary and a production/abandoned well close to the right boundary (Figure 1). All wells have uniform dimensions; however, a single perforation channel at the bottomhole is included in the injection well. The wells are spaced at a distance of 7 m (Table 2).

Initial and boundary conditions

The reservoir material consists of a single homogeneous formation material, which is initially unsaturated. This allows for the simulation of a single phase/single component flow process made up of CO₂ as the only fluid phase and a synthetic material, with similar properties to formation rocks, as the solid phase. In-situ stresses were developed as a result of boundary stresses applied in the vertical and lateral directions (Figure 1). These boundary stresses represent overburden and confining conditions that give rise to the initial and changing in-situ stresses within the formation. Walls of both wells are rigid and represent casings.

Loading

Fluid (CO₂) was introduced by injection at the bottomhole section of the injection well (Figure 2). Three test runs were conducted with changes made to the flow rate for each test. The injection flow rates applied include 0.5 m/s, 0.75 m/s and 1 m/s. All tests were run until stability in the occurrence of various key phenomena was achieved.

Spatial resolution

A (0.308 x 0.308) m grid size was used, constructed by discretising both flow domain and particle assembly into 26 x 39 active cells. The spatial resolution is given in terms of the ratio of grid size to particle size (G_{ratio}), where the size of the grid cell and particle size is denoted by the length and mean particle radius respectively. The G_{ratio} is hence denoted as

$$G_{ratio} = R_{av}^p / G_{size}$$

Where, R_{av}^p is the mean particle radius and G_{size} is the grid size given as the length. For a mean particle radius of 0.03 m, $G_{ratio} = 0.1$. According to a grid sensitivity analysis for a range of G_{ratio} between 0.042 and 0.250, there is no significant variance in results.

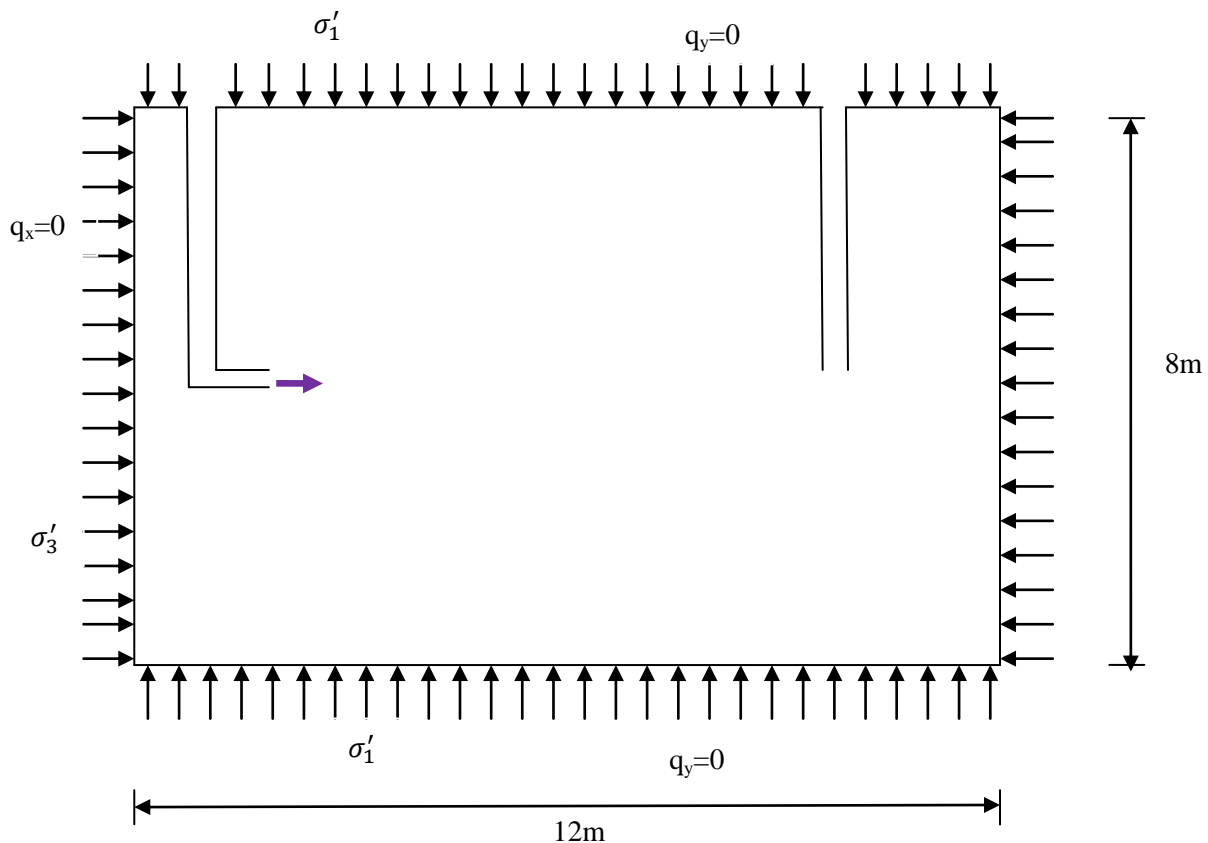


Fig 1 Reservoir model geometry/dimension

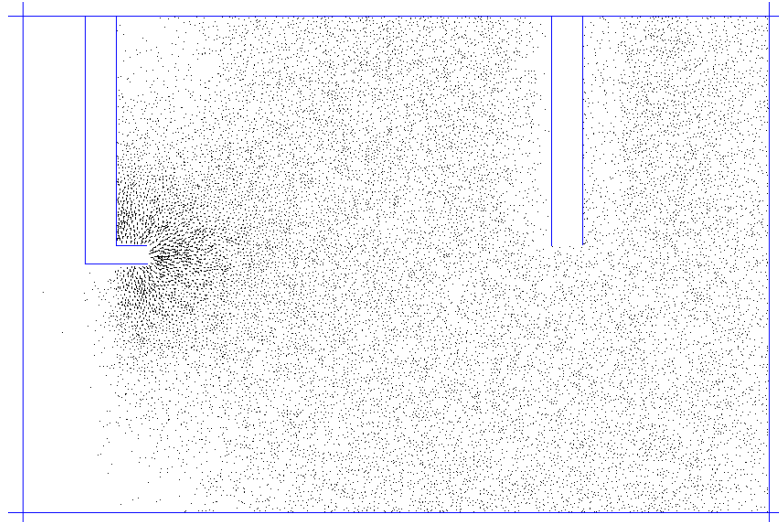


Fig 2 Velocity vectors showing the point of injection

Table 1 Micro-properties of rock material

Parameter	Description
Contact-bond normal strength (mean)	11.5MN/m ²
Contact-bond normal strength (std deviation)	2.845MN/m ²
Contact-bond shear strength	11.5MN/m ²
Contact-bond normal strength (std deviation)	2.845MN/m ²
Particle size (radius)	0.015m – 0.045m
Particle friction coefficient	1.0
Particle normal stiffness, k_n	29.0MN/m ²
Particle shear stiffness, k_s	10.36MN/m ²
Particle density	2650kg/m ³
Porosity	0.16
Particle-particle contact modulus	14.5GN/m ²
Particle stiffness ratio	2.8

Table 2 Mechanical properties and boundary conditions

Parameter Description	
Mechanical Properties	
Compressive strength q_c ,	17 MN/m ²
Elastic modulus, E	9.5 GN/m ²
Poisson ratio, $\hat{\nu}$	0.21
Boundary conditions	
Confining stress (vertical), σ_1	30.2 MN/m ²
Confining stress (lateral), σ_3	28.8 MN/m ²
Model dimensions	
Well diameter	0.5m
Distance between well point	7.0m

Table 3 Fluid properties

Parameter Description	
Viscosity	3.95e ⁻⁵ Pa-s
Density	479 Kg/m ³

3.0 Results and discussion

Comparisons were made in order to identify the controls within the reservoir system and to assess their contributing effect. The objective was to examine if the far reach wells could be affected by the fluid flow and fracturing process with respect to the following: the role played by operating variables such as the flow rate of injection and fluid pressure, the influence of the configuration of the well-reservoir system with respect to spatial distribution, the nature of occurring fractures and pattern of propagation, pressure build up around the zone of fluid injection as well as the far reach regions, pressure distribution between the injection and production/abandoned well and fluid velocity distribution between the injection point and far reach regions.

Figure 3 shows the early stage of fracture growth for an injection rate of 1 m/s, indicating an onset of fracturing caused by tensile failure at the vicinity of fluid injection. This is further buttressed in Figure 5 where a comparison is drawn between the rate of tensile and shear induced fracture growth. At the onset of fluid injection, drag forces as well as fluid pressure build-up eventually overcome the minimum principal stress as well as the tensile strength of the rock. The initial period of fracturing is therefore dominated by tensile induced cracks initiated around the edges of the perforation tunnel and extending mostly in the vertically upward and downward directions, which is also the direction of the minimum principal stress. Nevertheless, as fracturing progresses shear induced fractures become more prevalent (Figures 4-5) due to the weakening of the rock material and the vertical and horizontal confinement. The vertical confining stress represents the lithostatic (overburden) stress, while the horizontal confining stresses act as a result of the surrounding rock mass supposedly spread out infinitely away from both wells.

A similar pattern was observed when the fluid injection velocity was reduced to 0.75 m/s (Figures 6-7). Another area of semblance is the point of intersection between the tensile and shear curves that occurred when tensile fracturing attained a given magnitude; although the time of this incident was delayed when fluid was injected at the rate of 0.75 m/s. In other words, for both injection velocities (1 m/s and 0.75 m/s) tensile fracturing was dominant until a total magnitude of about 400 tensile cracks was formed. There was a point of inflexion signifying when shear fracturing begins to become proportionally greater than tensile fracture development (Figures 5 and 7) ; the implication of this is the occurrence of a similar trend in the fracturing process for fluid injection velocities within a given range. When the injection velocity was further reduced to 0.5m/s the rate of fracturing caused by tensile failure remained predominant throughout (Figures 8-9), because of the low extent of tensile and shear fracturing. Notwithstanding, if the duration of fluid injection is sufficiently protracted and provided there is a comparable magnitude of pressure build-up, it is assumed the same pattern will be observed.

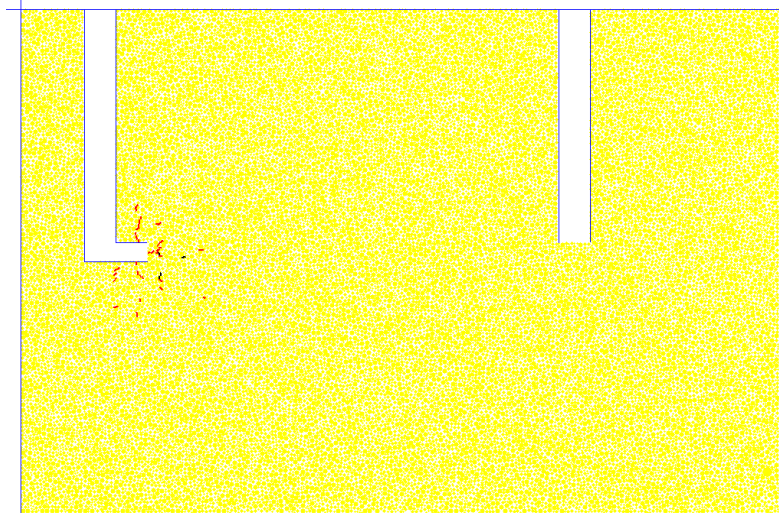


Fig 3 Onset of fracturing as fluid is introduced
(tensile fractures are shown in red)

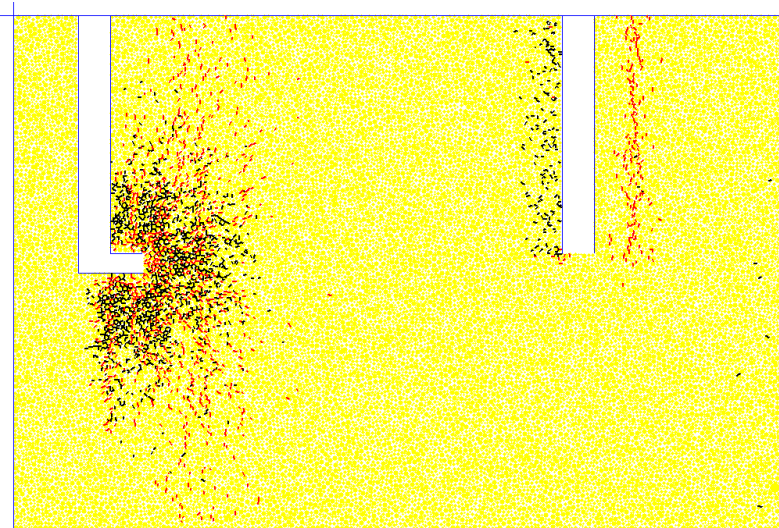


Fig 4 Pattern of fracture propagation due to fluid injection
(vel=1m/s)

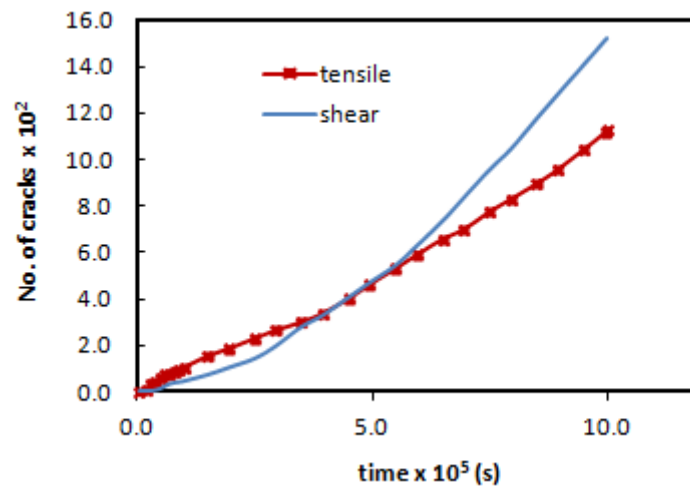


Fig 5 Tensile and shear fracture development
(vel=1m/s)

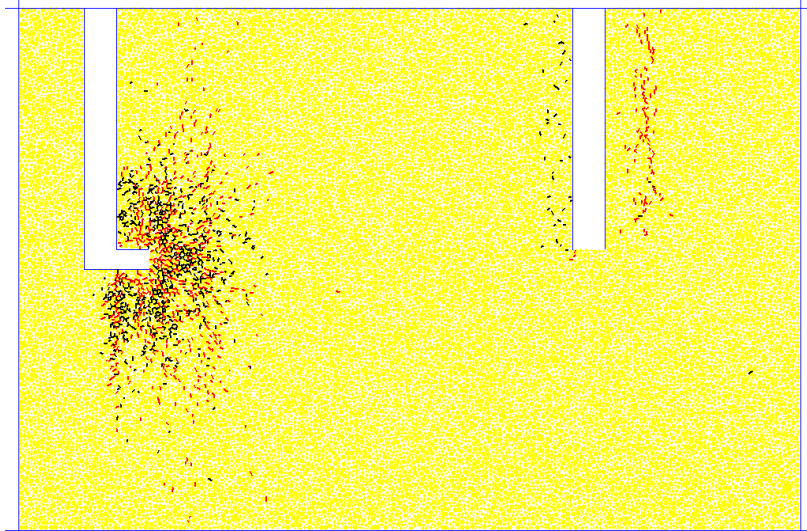


Fig 6 Pattern of fracture propagation due to fluid injection
(vel=0.75m/s)

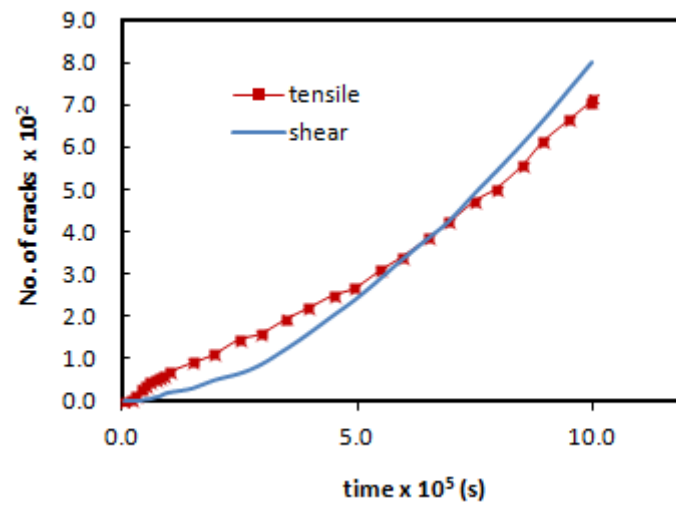


Fig 7 Tensile and shear fracture development
(vel=0.75m/s)

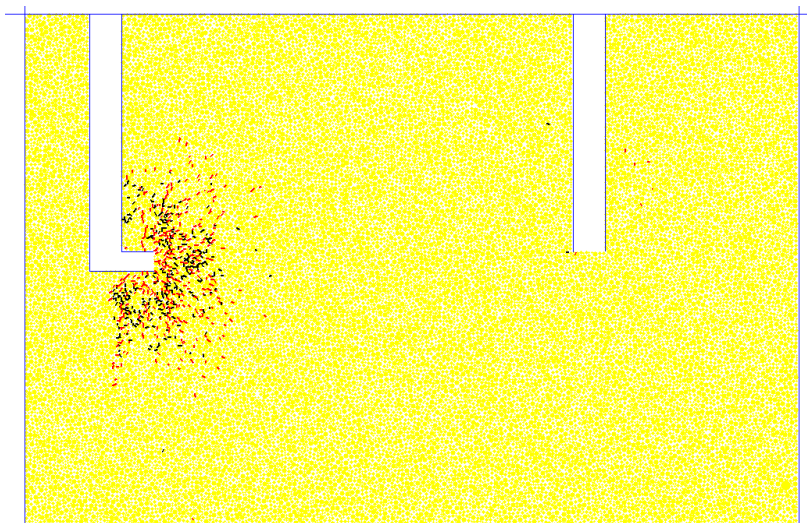


Fig 8 Pattern of fracture propagation due to fluid injection
(vel=0.5m/s)

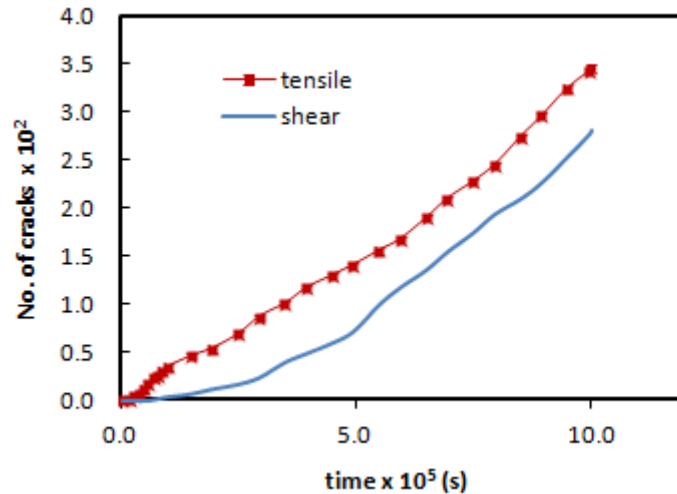


Fig 9 Tensile and shear fracture development
(vel=0.5m/s)

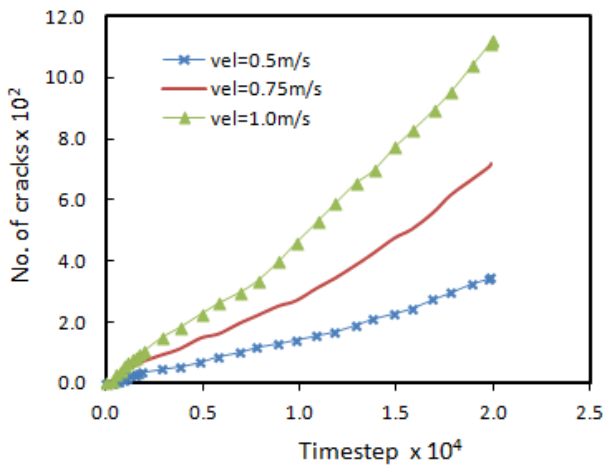
What happens at the far reach region is of paramount interest, especially when fluid is introduced from the injection well at a velocity sufficient to cause fracturing. As observed in Figures 4, 6 and 8 incidences of fracturing event take place at the far reach region, particularly at the proximity of the edges of the production/abandoned well, with the extent of fracturing becoming less severe with corresponding reductions in fluid injection velocity. For instance, when an injection velocity of 1 m/s was applied, the proliferation of fractures at the far reach well was very extensive (Figure 4), but when the injection velocity was lowered considerably to 0.5 m/s the extent of fracturing decreased (Figure 8). However, even at significantly low velocities, fracturing at far reach wells is anticipated to occur given sufficient elapse of time and pressure build-up.

An important feature to note is the nature of fracturing. As shown in Figures 4, 6, and 8, the mode of fracturing differ at both edges of the production/abandoned well. At the left well boundary, fracturing due to shear failure is prevalent and mainly caused by the restriction to the wall that prevents fluid flow and particle movement. Hence, the rock material around this zone has a propensity to fail due to shear and compressive stresses. This is not the case at the right well boundary. At this zone fracturing caused by tensile failure is observed and attributed to lesser restrictions on fluid flow and particle movement such that the drag force is able to exert a normal force sufficient to overcome the tensile strength of the rock material as well as the lateral confining stresses.

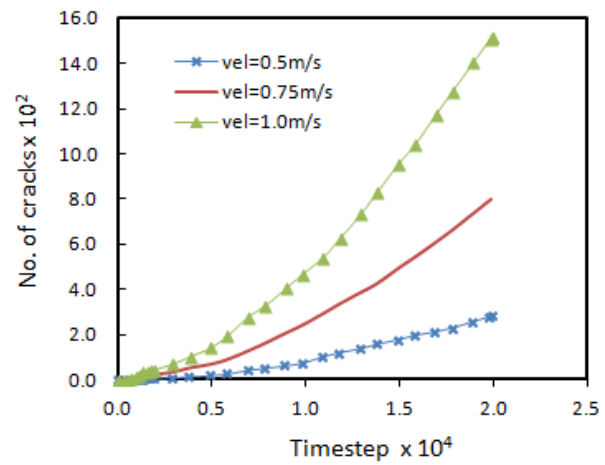
It is also vital to recognise that fractures occurring at the far reach well are not necessarily propagated from the injection point. In fact, as clearly seen in Figures 4, 6, and 8, there is no visible connection between the fracturing events occurring at the surrounds of the injection zone and the

fracturing events occurring at the vicinity of the production/abandoned well. This is a significant phenomenon that demonstrates the isolated effects that may possibly occur at a distant region even when fracturing caused by injecting fluid is seemingly localised at the area of injection. Thus it is feasible for fluid (in this case CO₂) injected through an injection well to enhance fracturing within the surrounds of a distant production/abandoned well which may consequently degrade the material strength of the rock mass, increasing its permeability which may lead to better oil recovery.

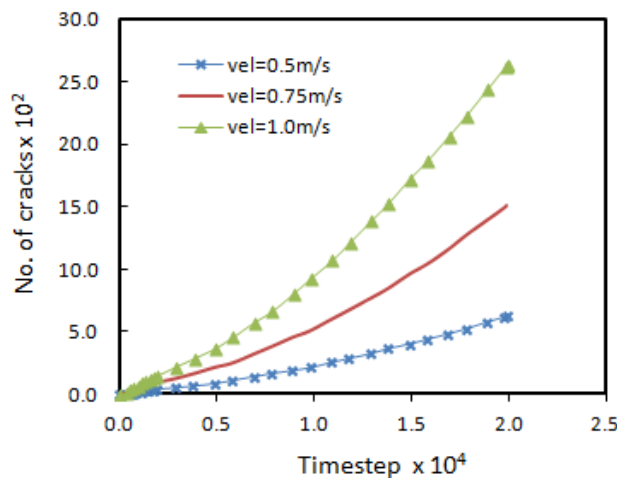
In Figures 10a-c the rate of development of tensile fractures (Figure 10a), shear fractures (Figure 10b) and total fractures (Figure 10c) are compared for various fluid injection velocities. As anticipated, the rate of fracture development as well as the magnitude of tensile, shear and total fractures is proportional to the magnitude of fluid injection velocity.



(10a) Magnitude of tensile fracturing at varying injection velocities



(10b) Magnitude of shear fracturing at varying injection velocities

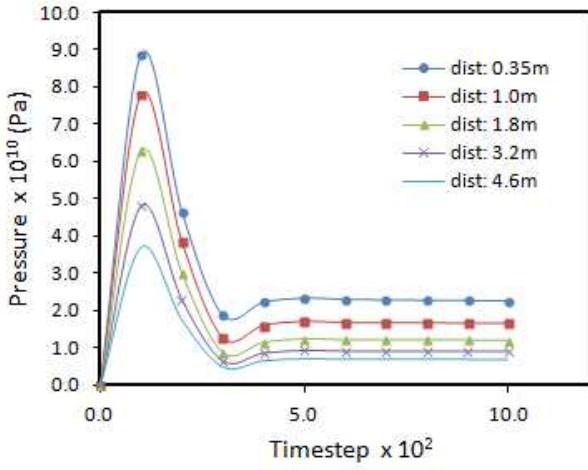


(10c) Magnitude of total fracturing at varying injection velocities

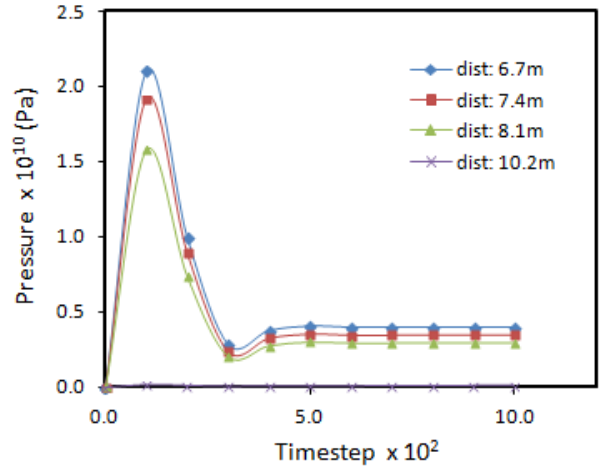
Fig 10 Magnitude fracturing at varying injection velocities

The pressure evolution near the injection well and the surrounds of the production/abandoned well for an injection velocity of 1 m/s is shown in Figures 11a and 11b respectively. Similar plots are also presented for the fluid injection velocity of 0.5 m/s (Figures 12a-12b). The trend of pressure development is similar to that earlier illustrated. They show an initial rise as the fluid pressure builds up, represented by a positive slope. After reaching a peak value there is a pressure drop (represented by a negative slope) which is subsequently followed by a regime where the pressure value becomes stable. Even though the trends of pressure history seem to be qualitatively identical for varying positions and fluid injection velocities, there are major differences in terms of the magnitude. For instance, when fluid is injected at a velocity of 1 m/s the peak pressure attained at just 0.35 m away from the injection point is exceedingly high (Figure 11a); however, for areas around the far reach well (production/abandoned well) the peak pressure is considerably lower (Figure 11b). Likewise, when the fluid injection velocity is lowered to 0.5 m/s, the peak pressure at 0.35 m from the point of injection is considerably lesser than is the case for higher injection velocities (Figure 12).

The magnitude and rate of pressure build up is strongly affected by the value of fluid injection rate and the location referenced from the point fluid is introduced, despite the semblance in trend (Figure 13). This fact is further illustrated in Figures 14a-b, where pressure profiles at different time periods and fluid injection velocities are depicted. There is a significant and almost linear drop in pressure away from the injection well. The same pattern occurs for decreasing injection rates. There is a substantial drop in pressure between 2.48 s and 3.48 s which corresponds to the period commencing from when the peak pressure is reached to when it becomes stable. In addition, a comparison of pressure profiles for varying fluid injection rates, as presented in Figure 15, shows a corresponding reduction in peak pressures with decreasing injection rate.

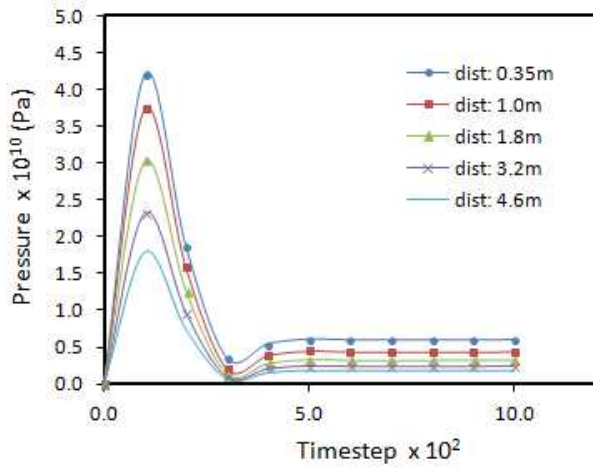


(11a) Pressure distribution near the injection well (vel=1m/s)

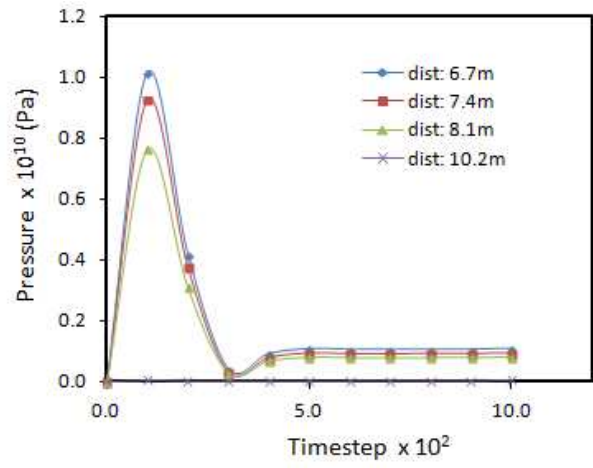


(11b) Pressure distribution at the far reach well (vel=1m/s)

Fig 11 Pressure distribution at the well vicinity (vel=1m/s)



(12a) Pressure distribution near injection well (vel=0.5m/s)



(12b) Pressure distribution at the far reach well (vel=0.5m/s)

Fig 12 Pressure distribution at the well vicinity (vel=0.5m/s)

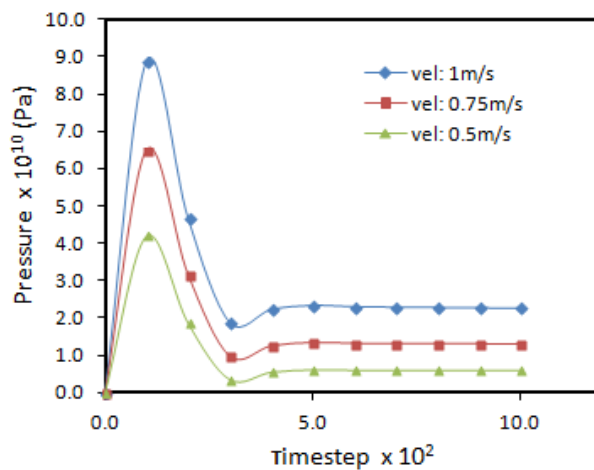
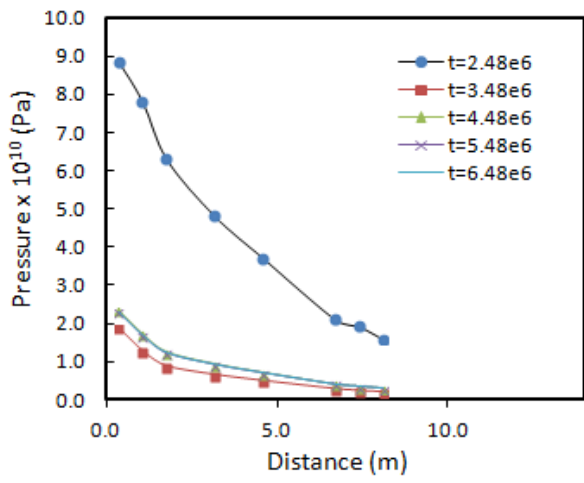
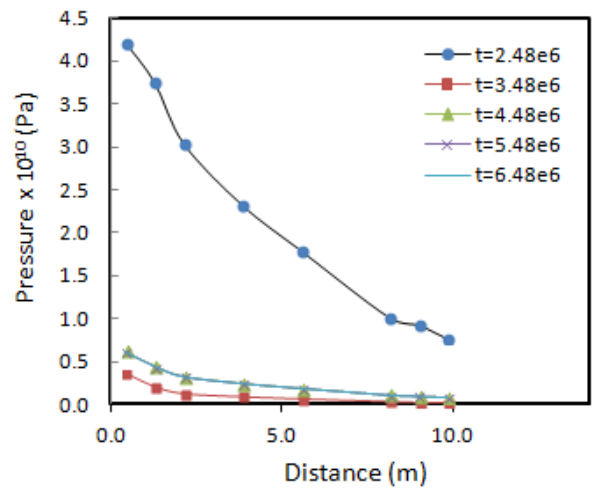


Fig 13 Comparison of pressure distribution for different injection rates (dist: 0.35m)



(14a) Pressure profile referenced from the injection well (vel=1m/s)



(14b) Pressure profile referenced from the injection well (vel=0.5m/s)

Fig 14 Pressure profile referenced from the injection well

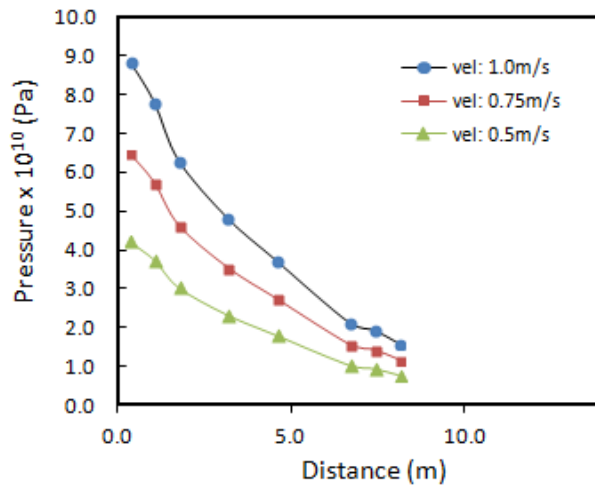
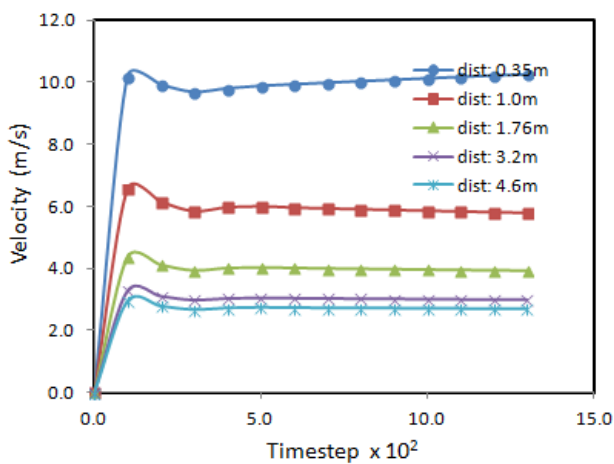


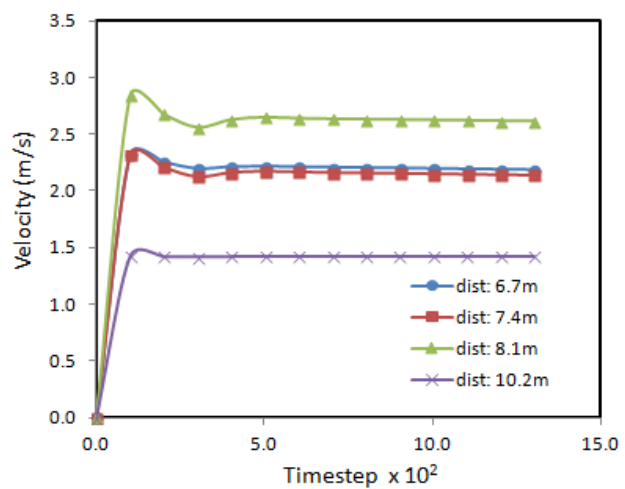
Fig 15 Peak pressure profile for different fluid injection rates

Records of the interstitial velocity were also measured as a function of time at varying positions referenced from the injection point. This was performed for different magnitudes of fluid injection rate (Figures 23-25). For each injection velocity, the interstitial velocities are several times higher in magnitude and are highly dependent on the permeability of the material, the porosity and the fluid viscosity.

The interstitial velocity, also referred to as the pore velocity, is related to the Darcy flux by the porosity. The Darcy flux represents the discharge rate and is divided by the porosity of the porous medium to account for the restrictions in flow within the material. Invariably, this results in an increase in fluid pressure at the pores. Figures 16-17 show an initial increase in interstitial velocities which become fairly stable for the rest of the test after reaching a maximum. The stretch of stable interstitial velocity values is much greater than the injection velocity (Figures 16-17) and indicates the non formation and growth of cavities irrespective of the high extent of fracturing. It is expected that a drop in interstitial velocities will occur at areas where there is cavity development, mainly due to the increase in void spaces.

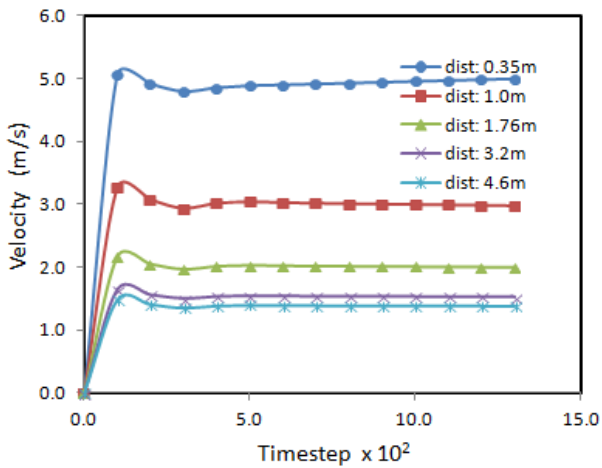


(16a) Velocity distribution near the injection well (vel=1m/s)

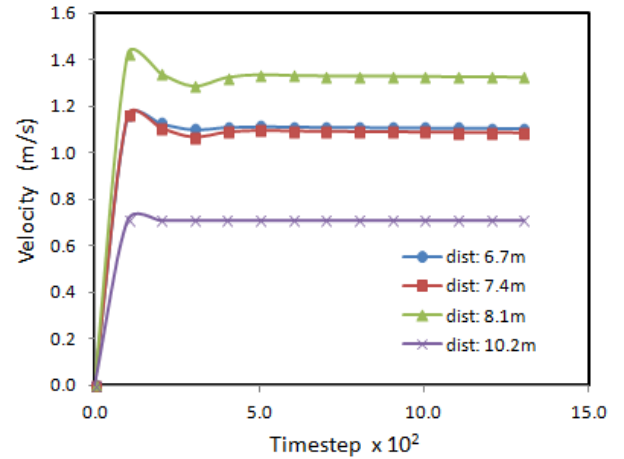


(16b) Velocity distribution at the far reach well (vel=1m/s)

Fig 16 Pore velocity distribution at the well vicinity (vel=1m/s)



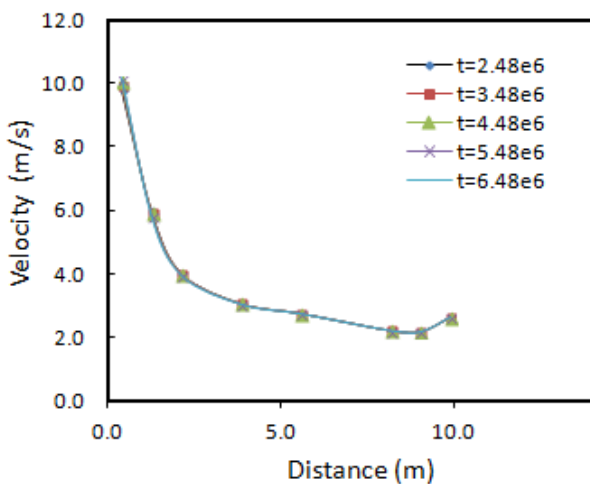
(17a) Velocity distribution near the injection well (vel=0.5m/s)



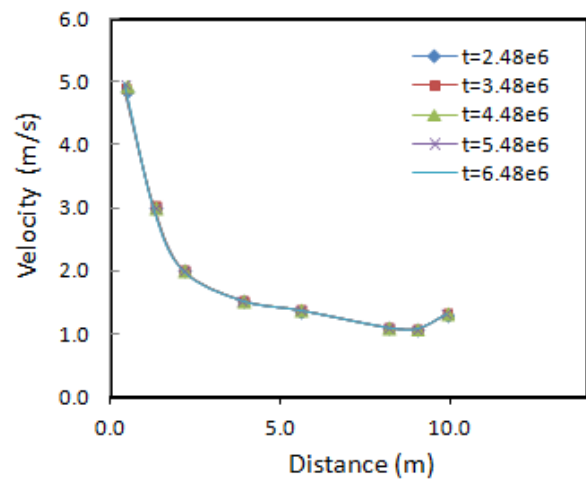
(17b) Velocity distribution at the far reach well (vel=0.5m/s)

Fig 17 Interstitial velocity distribution at the well vicinity (vel=0.5m/s)

Velocity profiles are presented in Figures 18a-b for various injection rates showing the spatial distribution of interstitial velocity at cumulative distances from the injection well. The pattern and magnitude remain consistent and independent of time. At regions closer to the injection well, there is a sharp drop in the interstitial velocity, but the gradient tends to become progressively flatter with distance. The velocity and pressure profiles exhibit analogous patterns, although the pressure profiles show a more linear relationship with distance. A comparison of velocity profiles at varying fluid injection rates (Figure 19) indicates a drop in interstitial velocities as the injection rate is decreased.



(18a) Interstitial velocity profile referenced from the injection well (vel=1m/s)



(18b) Interstitial velocity profile referenced from the injection well (vel=0.5m/s)

Fig 18 Interstitial velocity profile referenced from the injection well

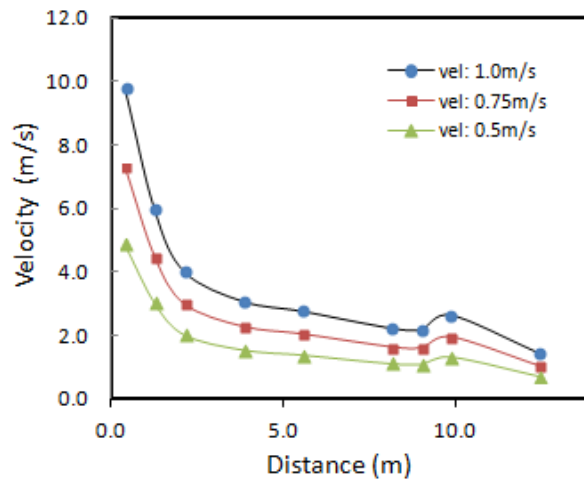


Fig 19 Interstitial velocity profile for different fluid injection rates

Conclusion

An alternative procedure to study the geo-mechanical changes that occur due to the injection of fluid at high flow rates into porous media has been presented. The DEM modelling technique was used to investigate the hydraulic fracturing processes as a result of fluid (CO_2) injection into a reservoir formation. The fracturing phenomenon was studied at the inter-particle level, with fracturing deemed to have occurred following the breakage of inter-particle bonds and/or detachment of particles. Simulation tests were conducted on a hypothetical well-reservoir system, simplified and representing a homogeneous reservoir formation comprising of two wells. The effects of operating variables such as injection flow rate and fluid pressure were investigated with emphasis on the nature of occurring fractures and pattern of propagation, pressure build up around the zone of fluid injection as well as the far reach regions, pressure distribution between the injection and production/abandoned well, and velocity distribution between the injection point and far reach regions. The Numerical test results show that for all cases the onset of fracturing is caused by tensile failure at the vicinity of fluid injection, as the drag forces and fluid pressure overcome both the tensile strength of the rock and the minimum principal stress. Hence, the first stage of fracturing which mainly occur at the edge of the perforation tunnel are instigated by tensile failure and as such dominated by tensile cracks. However, the cumulative impact of degradation of the rock mass combined with the confining effect of the boundary stresses lead to the generation of shear induced cracks which eventually become greater

than tensile induced cracks as a consequence of shear/compressive failure; this implies a prevalence of shear fracturing as the process continues.

An important highlight from the numerical results is the incidences of fracturing that occur at far reach wells as a result of fluid injection from a distant injection well. Depending on the fluid injection flow rate as well as the duration of injection, it is possible for fractures to occur at the proximity of edges of wells (such as production/abandoned wells) located at distant areas. There is a lack of physical connection between fracturing events at the injection region and the isolated fracturing that subsequently take place near the edges of the far reach well. Fractures that occur at far distant wells due to injection of fluid from an injection well are not necessarily propagated from the injection point.

As anticipated the rate of fracture development as well as the magnitude of tensile, shear and total fractures are directly associated with the magnitude of fluid injection velocity. In addition, the magnitude of pressure build-up is highly influenced by the fluid injection rate and the distance from the position of injection. The pressure gradient indicates a substantial and approximately linear drop in pressure when measured at intervals away from the injection point and a comparison of pressure profiles for varying fluid injection rates show a corresponding reduction in pressure with decreasing injection rates. Pore velocity profiling analysis also show non-linear but analogous patterns to pressure profiles. Unlike the pressure profile, the pattern and magnitude of pore velocity remain consistent and independent of time. Nevertheless, a comparison of pore velocity profiles at varying fluid injection rates indicates a drop in pore velocities as the injection rate decreases.

The modelling technique permits the dynamic monitoring of geo-mechanical changes projected from the particle level, thereby facilitating the observation of the influence of controlling factors that affect mechanisms governing the underground injection and storage of CO₂. Additional studies are essential for quantitative validations and applications to actual reservoir environments.

Acknowledgement

The first author acknowledges the funding of Petroleum Technology Development Fund (PTDF), Nigeria, throughout the duration of the research.

Abbreviations and Symbols

E	Elastic modulus
\vec{F}_i	Contact force (N)
\vec{F}_i^n	Normal component of contact force (N)
\vec{F}_i^s	Shear component of contact force (N)
K^n	Normal stiffness
k^s	Shear stiffness
\vec{U}_i^n	Normal component of contact displacement
$\Delta\vec{U}_i^s$	Increment in shear component of contact displacement
$\{\vec{F}_i^s\}_{rot2}$	Old shear force vector
$\Delta\vec{F}_i^s$	Shear elastic-increment vector
Δt	Timestep
t	Time
m	Particle mass
$\vec{\ddot{x}}_i$	Particle acceleration
\vec{g}_i	Body force acceleration
G_{ratio}	Ratio of grid size to particle size
G_{size}	Grid size
\vec{M}_i	Resultant moment
\vec{H}_i	Angular momentum
ρ_f	Fluid density
ϵ	Porosity
\vec{v}	Interstitial velocity
p	Fluid pressure
μ_f	Dynamic fluid viscosity

\vec{f}_b	Body force
\vec{f}_{drag}	Drag force from fluid
\vec{f}_{fluid}	Total force exerted by fluid on particle
\vec{u}	Average relative velocity between fluid and particles
R	Particle radius
R_{av}^p	Mean particle radius
q_c	Compressive strength
σ_1	Confining stress (vertical)
σ_3	Confining stress (lateral)
$\hat{\nu}$	Poisson ratio

References

- Al-Busaidi, A., Hazzard, J. F. and Young, R. P. 2005. Distinct element modeling of hydraulically fractured Lac du Bonnet granite. *Journal of Geophysical Research*, 110, B06302, doi:10.1029/2004JB003297.
- Al-Hashami, A., Ren, S. and Tohidi, B. 2005. CO₂ injection for enhanced gas recovery and geo-storage: reservoir simulation and economics *In: Proceedings of the SPE Europe/EAGE annual conference, SPE 94129, Madrid, PP 13-16.*
- Alqahtani, N. B. and Miskimins, J. L. 2010. 3D finite element modeling of laboratory hydraulic fracture experiments. *SPE EUROPE/EAGE Annual Conference and Exhibition in Barcelona, Spain, 14-17 June 2010.*
- Athavale, A. S. and Miskimins, J. L. 2008. Laboratory hydraulic fracturing on small homogeneous and laminated blocks. *42nd US Rock Mechanics Symposium, San Francisco June 29-July 2, 2008.*
- Bachu, S., Bonijoly, D., Bradshaw, J., Burruss, R., Holloway, S., Christensen, N. P. and Mathiassen, O. M. 2007. CO₂ storage capacity estimation: methodology and gaps. *International Journal of Greenhouse Gas Control*, 1, 430-443.
- Bachu, S., Shaw, J. C. and Pearson, R. M. 2004. Estimation of oil recovery and CO₂ storage capacity in CO₂ EOR incorporating the effect of underlying aquifers. *SPE/DOE Symposium on Improved Oil Recovery, 17-21 April 2004, Tulsa, Oklahoma.*

- Bauer, S., Class, H., Ebert, M., Feeser, V., Götze, H., Holzheid, A., Kolditz, O., Rosenbaum, S., Rabbel, W., Schäfer, D. and Dahmke, A. 2012. Modeling, parameterization and evaluation of monitoring methods for CO₂ storage in deep saline formations: the CO₂-MoPa project. *Environmental Earth Sciences*, 67, 351-367.
- Beyer, C., Li, D., Lucia, M., Kühn, M. and Bauer, S. 2012. Modelling CO₂-induced fluid–rock interactions in the Altensalzwedel gas reservoir. Part II: coupled reactive transport simulation. *Environmental Earth Sciences*, 67, 573-588.
- Birkholzer, J. T., Zhou, Q. L. and Tsang, C. F. 2009. Large-scale impact of CO₂ storage in deep saline aquifers: A sensitivity study on pressure response in stratified systems. *International Journal of Greenhouse Gas Control*, 3, 181-194.
- Blair, S. C., Thorpe, R. K., Heuze, F. E. and Shaffer, R. J. 1989. Laboratory observations of the effect of geologic discontinuities on hydrofracture propagation. *Rock Mechanics as a Guide for Efficient Utilization of Natural Resources*, Khair (ed.), Balkema, Rotterdam.
- Boone, T. J. and Ingraffea, A. R. 1990. A numerical procedure for simulation of hydraulically-driven fracture propagation in poroelastic media. *International Journal for Numerical and Analytical Methods in Geomechanics*, 14, 27-47.
- Boutt, D. F., Cook, B. K., McPherson, B. J. O. L. and Williams, J. R. 2007. Direct simulation of fluid-solid mechanics in porous media using the discrete element and lattice-Boltzmann methods. *Journal of Geophysical Research*, 112, B10209, doi: 10.1029/2004JB003213.
- Boutt, D. F., Cook, B. K. and Williams, J. R. 2011. A coupled fluid-solid model for problems in geomechanics: Application to sand production. *International Journal for Numerical and Analytical Methods in Geomechanics*, 35, 997-1018.
- Bradshaw, J., Bachu, S., Bonijoly, D., Burruss, R., Holloway, S., Christensen, N. P. and Mathiassen, O. M. 2007. CO₂ storage capacity estimation: Issues and development of standards. *International Journal of Greenhouse Gas Control*, 1, 62-68.
- Casas, L., Miskimins, J. L., Black, A. and Green, S. 2006. Laboratory hydraulic fracturing test on a rock with artificial discontinuities. *SPE Annual Technical Conference and Exhibition, San Antonio, Texas, USA 24-27 September 2006*
- Class, H., Ebigbo, A., Helmig, R., Dahle, H. K., Nordbotten, J. M., Celia, M. A., Audigane, P., Melanie, D., Ennis-King, J., Fan, Y., Flemisch, B., Gasda, S. E., Jin, M., Krug, S., Labregere, D., Beni, A. N., Pawar, R. J., Sbai, A., Thomas, S. G., Trenty, L. and Wei, L. 2009. A benchmark study on problems related to CO₂ storage in geologic formations. *Computational Geosciences*, 13, 409-434.
- Daneshy, A. A. 1976. Rock properties controlling hydraulic fracture propagation. *SPE-European Spring Meeting of Society of Petroleum Engineers of American Institute of Mining, Metallurgical, and Petroleum Engineers (SPE-AIME), Amsterdam, Netherlands, April 8-9, 1976* [Online].

- Daneshy, A. A. 1978. Hydraulic fracture propagation in layered formations. *Spe Journal*, 18, 33-41.
- Dean, R. H. and Schmidt, J. H. 2009. Hydraulic fracture predictions with a fully coupled geomechanical reservoir simulator. *Spe Journal*, 14 (4), 707-714.
- Eigestad, G. T., Dahle, H. K., Hellevang, B., Riis, F., Johansen, W. T. and Oian, E. 2009. Geological modeling and simulation of CO₂ injection in the Johansen formation. *Computational Geosciences*, 13, 435-450.
- El Shamy, U. and Zeghal, M. 2005. Coupled continuum-discrete model for saturated granular soils. *Journal of Engineering Mechanics*, 131 (4), 413-426.
- Elwood, D. and Moore, I. 2009. Hydraulic fracturing experiments in sand and gravel and approximations for maximum allowable mud pressure. *The North American Society (NASTT) and the International Society for Trenchless Technology (ISTT) International No-Dig Show 2009*.
- Eshiet, K. and Sheng, Y. 2013. Investigation of geomechanical responses of reservoirs induced by carbon dioxide storage. *Environmental Earth Sciences*, 1-22.
- Eshiet, K., Sheng, Y. and Ye, J. 2013. Microscopic modelling of the hydraulic fracturing process. *Environmental Earth Sciences*, 68, 1169-1186.
- Fjaer, E., Holt, R. M., Horsrud, P., Raaen, A. M. and Risnes, R. 2008. Petroleum related rock mechanics. *Developments in Petroleum Science*, 53, 2nd Edition. Elsevier, UK.
- Godec, M. L., Kuuskraa, V. A. and Dipietro, P. 2013. Opportunities for Using Anthropogenic CO₂ for Enhanced Oil Recovery and CO₂ Storage. *Energy & Fuels*, 27, 4183-4189.
- Gozalpour, F., Ren, S. R. and Tohidi, B. 2005. CO₂ EOR and storage in oil reservoirs. *Oil & Gas Science and Technology – Rev. IFP*, 60 (3) 537-546.
- Hanson, M. E., Anderson, G. D., Shaffer, R. J. and Thorson, L. D. 1982. Some effects of stress, friction, and fluid flow on hydraulic fracturing. *Society of Petroleum Engineers Journal*, 22, 321-332.
- Hanson, M. E., Shaffer, R. and Anderson, G. D. 1981. Effects of various parameters on hydraulic fracturing geometry. *SPE Journal*, 21, 435-443.
- Hoffman, B. T. and Chang, W. M. 2009. Modeling hydraulic fractures in finite difference simulators: Application to tight gas sands in Montana. *Journal of Petroleum Science and Engineering*, 69, 107-116.
- Hou, Z., Gou, Y., Taron, J., Gorke, U. and Kolditz, O. 2012. Thermo-hydro-mechanical modeling of carbon dioxide injection for enhanced gas-recovery (CO₂-EGR): a benchmarking study for code comparison. *Environmental Earth Sciences*, 67, 549-561.

- Huq, F., Blum, P., Marks, M. W., Nowak, M., Haderlein, S. and Grathwohl, P. 2012. Chemical changes in fluid composition due to CO₂ injection in the Altmark gas field: preliminary results from batch experiments. *Environmental Earth Sciences*, 67, 385-394.
- Ishida, T. 2001. Acoustic emission monitoring of hydraulic fracturing in laboratory and field. *Construction and Building Materials*, 15, 283-295.
- Ishida, T., Chen, Q., Mizuta, Y. and Roegiers, J.-C. 2004. Influence of fluid viscosity on the hydraulic fracturing mechanism. *Journal of Energy Resources Technology*, 126, 190-200.
- Itasca Consulting Group 2008. PFC 2D (Particle Flow Code, 2 dimension), version 4.0 user manual. Minneapolis, Minnesota.
- Jansen, J.-D., van den Hoek, P. J., Zwarts, D., Al-Masfry, R., Hustedt, B. and van Schijndel, L. 2008. Behaviour and impact of dynamic induced fractures in waterflooding and EOR. *The 42nd U.S. Rock Mechanics Symposium (USRMS), June 29 - July 2, 2008*. San Francisco, CA: American Rock Mechanics Association.
- Kopp, A., Class, H. and Helmig, R. 2009. Investigations on CO₂ storage capacity in saline aquifers- Part 2: Estimation of storage capacity coefficients. *International Journal of Greenhouse Gas Control*, 3, 277-287.
- Kühn, M., Tesmer, M., Pilz, P., Meyer, R., Reinicke, K., Förster, A., Kolditz, O. and Schäfer, D. 2012. CLEAN: project overview on CO₂ large-scale enhanced gas recovery in the Altmark natural gas field (Germany). *Environmental Earth Sciences*, 67, 311-321.
- Lam, K. Y. and Cleary, M. P. 1986. A complete three-dimensional simulator for analysis and design of hydraulic fracturing. *SPE Unconventional Gas Technology Symposium, Louisville, KY, May 18-21, 1986*.
- Lempp, C., Shams, K. and Jahr, N. 2012. Approaches to stress monitoring in deep boreholes for future CCS projects. *Environmental Earth Sciences*, 67, 435-445.
- Liao, X. W. and Shangguan, Y. N. 2009. Research of the estimation method of CO₂ saline aquifer storage capacity. *Asia-Pacific Power and Energy Engineering Conference (Appeec), Vols 1-7*, 3143-3149.
- Lindeberg, E. and Bergmo, P. 2003. The long-term fate of CO₂ injected into an aquifer. *Greenhouse Gas Control Technologies, Vols I and II, Proceedings*, 489-494.
- Lucia, M., Bauer, S., Beyer, C., Kühn, M., Nowak, T., Pudlo, D., Reitenbach, V. and Stadler, S. 2012. Modelling CO₂-induced fluid-rock interactions in the Altensalzwedel gas reservoir. Part I: from experimental data to a reference geochemical model. *Environmental Earth Sciences*, 67, 563-572.
- Lujun, J., Settari, A. and Sullivan, R. B. 2009. A Novel hydraulic fracturing model fully coupled with geomechanics and reservoir simulation. *Spe Journal*, 14 (3), 423-430.

- Mathias, S. A., Hardisty, P. E., Trudell, M. R. and Zimmerman, R. W. 2009b. Screening and selection of sites for CO₂ sequestration based on pressure buildup. *International Journal of Greenhouse Gas Control*, 3, 577-585.
- Matsunaga, I., Kobayashi, H. and Ishida, T. 1993. Studying hydraulic fracturing mechanism by laboratory experiments with acoustic emission monitoring. *International Journal of Rock Mechanics and Mining Science & Geomechanics*, 30, 909-912.
- McLennan, J. D., Hasegawa, H. S., Roegiers, J. C. and Jessop, A. M. 1986. Hydraulic fracturing experiments at the University of Regina campus. *Can. Geotech. J.*, 23, 548-555.
- Medlin, W. L. and Masse, L. 1984. Laboratory experiments in fracture propagation. *Society of Petroleum Engineers Journal*, 24.
- Murdoch, L. C. 1993a. Hydraulic fracturing of soil during experiments, Part I Methods and Observations. *Geotechnique*, 43, 255-265.
- Murdoch, L. C. 1993b. Hydraulic fracturing of soil during experiments, Part II Propagation. *Geotechnique*, 43, 267-276.
- Murdoch, L. C. 1993c. Hydraulic fracturing of soil during experiments, Part III Theoretical Analysis. *Geotechnique*, 43, 277-287.
- Nicot, J.-P., Hovorka, S. D. and Choi, J.-W. 2009. Investigation of water displacement following large CO₂ sequestration operations. *Energy Procedia*, 1, 4411-4418.
- Nicot, J. P. 2008. Evaluation of large-scale CO₂ storage on fresh-water sections of aquifers: an example from the Texas Gulf Coast Basin. *International Journal of Greenhouse Gas Control*, 2 (4), 582-593.
- Nordbotten, J. M., Celia, M. A. and Bachu, S. 2005a. Injection and storage of CO₂ in deep saline aquifers: Analytical solution for CO₂ plume evolution during injection. *Transport in Porous Media*, 58, 339-360.
- Nordbotten, J. M., Celia, M. A., Bachu, S. and Dahle, H. K. 2005b. Semianalytical solution for CO₂ leakage through an abandoned well. *Environmental Science & Technology*, 39, 602-611.
- Nordbotten, J. M., Kavetski, D., Celia, M. A. and Bachu, S. 2009. Model for CO₂ leakage including multiple geological layers and multiple leaky wells. *Environmental Science & Technology*, 43 (3), 743-749.
- Norden, B., Förster, A., Behrends, K., Krause, K., Stecken, L. and Meyer, R. 2012. Geological 3-D model of the larger Altensalzwedel area, Germany, for temperature prognosis and reservoir simulation. *Environmental Earth Sciences*, 67, 511-526.

- Nunez-Lopez, V., Holtz, M. H., Wood, D. J., Ambrose, W. A. and Hovorka, S. D. 2008. Quick-look assessments to identify optimal CO₂ EOR storage sites. *Environmental Geology*, 54, 1695-1706.
- Okwen, R. T., Stewart, M. T. and Cunningham, J. A. 2010. Analytical solution for estimating storage efficiency of geologic sequestration of CO₂. *International Journal of Greenhouse Gas Control*, 4, 102-107.
- Papanastasiou, P. C. 1997. A coupled elastoplastic hydraulic fracturing model. *Int. J. Rock Mech & Min. Sci.*, 34 (3-4), 240.e1–240.e15.
- Park, Y.-C., Huh, D.-G. and Park, C.-H. 2012. A pressure-monitoring method to warn CO₂ leakage in geological storage sites. *Environmental Earth Sciences*, 67, 425-433.
- Parrish, R. L., Stevens, A. L. and Turner Jr., T. F. 1981. A true in-situ fracturing experiment - Final results. *Journal of Petroleum Technology*.
- Pini, R., Storti, G. and Mazzotti, M. 2011. A model for enhanced coal bed methane recovery aimed at carbon dioxide storage. *Adsorption-Journal of the International Adsorption Society*, 17, 889-900.
- Pruess, K. 2008a. Leakage of CO₂ from geologic storage: role of secondary accumulation at shallow depth *International Journal of Greenhouse Gas Control*, 2, 37-46.
- Pruess, K. 2008b. On CO₂ fluid flow and heat transfer behavior in the subsurface, following leakage from a geologic storage reservoir. *Environmental Geology*, 54, 1677-1686.
- Pudlo, D., Reitenbach, V., Albrecht, D., Ganzer, L., Gernert, U., Wienand, J., Kohlhepp, B. and Gaupp, R. 2012. The impact of diagenetic fluid–rock reactions on Rotliegend sandstone composition and petrophysical properties (Altmark area, central Germany). *Environmental Earth Sciences*, 67, 369-384.
- Rungamornrat, J., Wheeler, M. F. and Mear, M. E. 2005. Coupling of fracture/non-newtonian flow for simulating nonplanar evolution of hydraulic fractures. *SPE Annual Technical Conference and Exhibition, 9-12 October*. Dallas, Texas.
- Rutqvist, J., Birkholzer, J., Cappa, F. and Tsang, C. F. 2007. Estimating maximum sustainable injection pressure during geological sequestration of CO₂ using coupled fluid flow and geomechanical fault-slip analysis. *Energy Conversion and Management*, 48, 1798-1807.
- Rutqvist, J., Birkholzer, J. and Tsang, C. F. 2008. Coupled reservoir-geomechanical analysis of the potential for tensile and shear failure associated with CO₂ injection in multilayered reservoir-caprock systems. *International Journal of Rock Mechanics & Mining Sciences*, 45, 132-143.

- Shimizu, H., Murata, S. and Ishida, T. 2009. The distinct element analysis for hydraulic fracturing considering the fluid viscosity. *43rd US Rock Mechanics Symposium and 4th US-Canada Rock Mechanics Symposium. June 28th – July 1, 2009. Asheville, NC.*
- Shimizu, H., Murata, S. and Ishida, T. 2011. The distinct element analysis for hydraulic fracturing in hard rock considering fluid viscosity and particle size distribution. *International Journal of Rock Mechanics and Mining Science & Geomechanics* 48, 712-727.
- Singh, A. K., Baumann, G., Henniges, J., Görke, U. J. and Kolditz, O. 2012. Numerical analysis of thermal effects during carbon dioxide injection with enhanced gas recovery: a theoretical case study for the Altmark gas field. *Environmental Earth Sciences*, 67, 497-509.
- Streit, E. E. and Hillis, R. R. 2004. Estimating fault stability and sustainable fluid pressures for underground storage of CO₂ in porous rock. *Energy*, 29, 1445-1456.
- Streit, J. E. 2002. Estimating fluid pressures that can induce reservoir failure during hydrocarbon depletion. *SPE/SRM Rock Mechanics Conference , Irving, Texas, 20-23 October.*
- Teufel, L. W. and Clark, J. A. 1984. Hydraulic fracture propagation in layered rock: experimental studies of fracture containment. *Spe Journal*, 24 (1), 19-32.
- Warpinski, N. R., Clark, J. A., Schmidt, R. A. and Huddle, C. W. 1982. Laboratory investigation on the effect of in-Situ stresses on hydraulic fracture containment. *SPE Journal* 22 (3), 333-340.
- Wei, L. L. and Saaf, F. 2009. Estimate CO₂ storage capacity of the Johansen formation: numerical investigations beyond the benchmarking exercise. *Computational Geosciences*, 13, 451-467.
- Xu, T. F., Sonnenthal, E., Spycher, N. and Pruess, K. 2006. TOUGHREACT - A simulation program for non-isothermal multiphase reactive geochemical transport in variably saturated geologic media: Applications to geothermal injectivity and CO₂ geological sequestration. *Computers & Geosciences*, 32, 145-165.
- Yamamoto, K., Shimamoto, T. and Maezumi, S. 1999. Development of a true 3D hydraulic fracturing simulator. *SPE Asia Pacific Oil and Gas Conference and Exhibition, Jakarta, Indonesia, 20-22 April*
- Yew, C. H. and Liu, G. F. 1993. Fracture tip and critical stress intensity factor of a hydraulically induced fracture. *SPE Production and Facilities* 8 (3), 171-177.
- Zhang, B. B. and Song, X. C. 2012. Geological Storage of CO₂ to Enhance Coalbed Methane Production. In: WU, J., YANG, J., NAKAGOSHI, N., LU, X. & XU, H. (eds.) *Natural Resources and Sustainable Development li, Pts 1-4.*
- Zhou, Q. L., Birkholzer, J. T., Tsang, C. F. and Rutqvist, J. 2008. A method for quick assessment of CO₂ storage capacity in closed and semi-closed saline formations. *International Journal of Greenhouse Gas Control*, 2, 626-639.